
This is an electronic reprint of the original article.
This reprint may differ from the original in pagination and typographic detail.

Holmberg, Nico; Laasonen, Kari

Ab Initio Electrochemistry: Exploring the Hydrogen Evolution Reaction on Carbon Nanotubes

Published in:
Journal of Physical Chemistry C

DOI:
[10.1021/acs.jpcc.5b04739](https://doi.org/10.1021/acs.jpcc.5b04739)

Published: 01/01/2015

Document Version
Peer-reviewed accepted author manuscript, also known as Final accepted manuscript or Post-print

Please cite the original version:
Holmberg, N., & Laasonen, K. (2015). Ab Initio Electrochemistry: Exploring the Hydrogen Evolution Reaction on Carbon Nanotubes. *Journal of Physical Chemistry C*, 119(28), 16166-16178.
<https://doi.org/10.1021/acs.jpcc.5b04739>

This material is protected by copyright and other intellectual property rights, and duplication or sale of all or part of any of the repository collections is not permitted, except that material may be duplicated by you for your research use or educational purposes in electronic or print form. You must obtain permission for any other use. Electronic or print copies may not be offered, whether for sale or otherwise to anyone who is not an authorised user.

This document is the Accepted Manuscript version of a Published Work that appeared in final form in the Journal of Physical Chemistry C, copyright © American Chemical Society after peer-review and technical editing by the publisher.

To access the final edited and published work see <http://pubs.acs.org/doi/abs/10.1021/acs.jpcc.5b04739>

J. Phys. Chem. C, 2015, 119 (28), pp 16166–16178, DOI: 10.1021/acs.jpcc.5b04739

Ab Initio Electrochemistry: Exploring the Hydrogen Evolution Reaction on Carbon Nanotubes

Nico Holmberg, and Kari Laasonen*

COMP Centre of Excellence in Computational Nanoscience, Department of Chemistry, Aalto University, P.O. Box 16100, FI-00076 Aalto, Finland

E-mail: kari.laasonen@aalto.fi

*To whom correspondence should be addressed

Abstract

Density functional theory (DFT) was employed to investigate the hydrogen evolution reaction (HER) on pristine and nitrogen doped carbon nanotubes (CNTs) in acidic solution. As the reaction is an electrocatalytic surface reaction, an accurate description of HER requires performing simulations under constant electrode potential conditions. To this end, we examined HER at several electrode charges allowing us to determine grand canonical activation energies as a continuous function of electrode potential. By studying the elementary steps of HER – the Volmer, Tafel and Heyrovsky reactions – and by considering hydrogen coverage effects, we found that the Volmer-Heyrovsky mechanism is the predominant HER mechanism on CNTs with the Heyrovsky step being rate-determining. Our results indicated that CNTs are electrochemically active towards HER, which seen as a decrease in activation energies with growing electrode potential, but that the activity is lower than on platinum matching experimental data. Substitutional nitrogen doping did not improve HER activity, and further research is required to determine which nitrogen configurations contribute to the enhanced catalytic activity observed for experimental NCNTs.

Keywords

Density functional theory, electrocatalysis, nudged elastic band method, molecular dynamics

1 Introduction

Density functional theory (DFT) has successfully been applied to a wide variety of topics in chemistry ranging from heterogeneous surface catalysis¹ to complex reactions in solution.² A field of chemistry that has received far less attention is electrochemistry and, in particular, electrocatalytic reactions at electrolyte-electrode interfaces, despite their importance in e.g. modern day electronics. The major difference between chemical catalysis and electrocatalysis is that the latter always includes an electron transfer (ET) reaction in addition to any chemical changes.

Describing ET reactions with time-independent DFT faces two main obstacles. The first is related to the use of generalized gradient approximations (GGA) for the DFT exchange-correlation (XC) interaction, which causes electron density to become overly delocalized.³ This prohibits, for instance, the simulation of ET reactions between solvated ions. While more accurate XC functionals are a natural solution to the problem, computationally less-demanding methods, such as charge constrained DFT,⁴ have been demonstrated to be a viable alternative. The second issue, namely, the lack of control over the computational electrode potential, is a more severe problem in the study of electrocatalytic surface reactions. In contrast to experiments, the electrode potential cannot be fixed to a finite value because the number of electrons is fixed in traditional DFT implementations. When combined with the limited system sizes that can be treated with present computational resources, an inevitable side effect of any electrochemical reaction is a considerable shift in the electrode potential, obscuring comparison to experimental data.

Several methods^{5–13} have been proposed for correcting quantum chemical calculations to constant electrode potential. The most elegant solution would be to treat electrons in the grand canonical ensemble, that is, to allow the number of electrons to change during the electronic structure self-consistency loop, which is equivalent to connecting the system to a fictitious potentiostat.^{5,6} Unfortunately, convergence of the grand canonical Kohn-Sham equations is significantly slower than with a fixed number of electrons, limiting the method to small system sizes. Other suggested methods rely on extrapolating calculated energies from canonical, constant charge DFT simulations to constant electrode potential. Rossmeisl et al.⁷ have shown how reactions modeled with different supercell sizes can be used to recover activation energies in the limit of infinite system size, where the shift in potential vanishes. In this method, the electrode potential is controlled indirectly by varying the concentration of solvated protons. In a different approach, Neurock and Filhol^{8,9} proposed controlling the electrode potential by adding or removing electrons from the electrode, enabling the calculation of absolute energies on a continuous potential scale using a single supercell size. Numerous variants^{10–12} to this method have been suggested, which mainly differ in the treatment of the electrolyte or the electrode counter-charge. Recently, the method has

also been extended to grand canonical simulations in the framework of joint-density functional theory.¹³ For a detailed overview of the presented methods including suggestions for further improvements, we refer the interested reader to ref. 14.

Here, we propose a modification of the Neurock and Filhol method for studying electrochemical reactions under constant potential conditions. As an example system, we consider the hydrogen evolution reaction on pristine and nitrogen doped carbon nanotubes, which belong to a widely studied class of materials in the development of metal-free alternatives to platinum for sustainable hydrogen production. To our knowledge, with the exception of the pioneering work of Skúlason et al.¹⁵ on platinum surfaces and Taylor and co-workers¹⁶ on Ni(111), this is the first time that the electrode potential dependence of HER is determined in a rigorous manner. While previous studies^{17,18} of HER on CNTs do include calculations with varying surface charge, we show that it is necessary to correct for changes in the electrode potential during HER to obtain a quantitatively accurate description of the reaction's potential dependence.

In acidic solution, HER corresponds to the net reduction of two protons into molecular hydrogen



It is generally accepted that HER occurs via two competing mechanisms. These so-called Volmer-Heyrovsky and Volmer-Tafel mechanisms are comprised of the elementary reactions



where H^* denotes adsorbed hydrogen atoms. Depending on catalyst, one of the mechanisms is often favored and dominates the total electrocatalytic rate.

This paper is divided as follows. First, we give an overview of our methodology for calculating electrode potentials and determining potential dependent, grand canonical activation energies. Details of the performed calculations are also presented. Next, we verify the accuracy of our electrode-electrolyte model at charge neutral conditions by calculating the nanotube potential of zero charge using ab initio molecular dynamics. We then explore both mechanisms of HER on nitrogen doped and pristine carbon nanotubes and quantify the effects of substitutional nitrogen doping. From the calculated minimum energy profiles, we conclude that the Volmer-Heyrovsky mechanism is the predominant HER mechanism and subsequently analyze how the activation energies of this mechanism depend on electrode potential, enabling direct comparison with experimental data. Lastly, we discuss how the calculated HER barriers depend on the surface coverage of adsorbed hydrogen atoms.

2 Theoretical Methods

2.1 Electrode Potential

The potential of a metallic electrode can be controlled directly by varying the total number of electrons N within the system while keeping the number of atoms constant. In practice, the excess electrons are added to (or withdrawn from) energy levels close to the electrode Fermi level μ , which simultaneously shifts the Fermi level and hence the electrode potential. This procedure also induces a surface charge on the electrode. As periodic systems cannot possess a net charge q , the charge on the electrode needs to be compensated by a counter-charge with opposite sign. For this purpose, we used a homogeneous background counter-charge, which is applied implicitly during the evaluation of the total electrostatic energy using Ewald summation by omitting the $\mathbf{G} = 0$ term when the reciprocal-space electron density is Fourier transformed to real-space (see e.g. ref. 19 or 20).

The relation between electrode Fermi level and potential is realized by using Trasatti's²¹ definition of absolute electrode potentials. To use this definition, we consider an electrode fully

immersed in solution, where the periodic copies of the system are separated by vacuum in the directions perpendicular to the electrode, see Figure 2. The absolute electrode potential, $U_0^{abs.}$, of an uncharged electrode can be calculated from²²

$$U_0^{abs.} = \frac{-\mu + e\phi_0}{e} := \frac{\Phi_0}{e} \quad (2)$$

where e is the elementary charge and ϕ_0 is the Volta (outer) potential outside the solvent layer in vacuum. We have further assumed that the Fermi level μ is given in units of electron volt. Formally, the Volta potential multiplied by the elementary charge is a measure of the work required to transport an electron at rest in vacuum to a point just outside the solution. However, as pointed out by Tripkovic et al.,²³ the concept of an absolute vacuum reference is ill-defined in periodic DFT calculations and the only valid zero level for electron energies is an electron in vacuum just outside the solution. This also implies that the Fermi level should be referenced to the average electrostatic potential at this point redefining the Volta potential in Eq. 2 (see below for details on numerical evaluation). Analogously, the term Φ_0 can be interpreted as the work function of the solvated electrode, i.e., as the energy required to remove an electron from the metal Fermi level and transport it through the solvent to vacuum outside the solvent. In the absence of solution, Φ_0 is equivalent to the standard definition of vacuum work functions. For an in-depth review of electrochemical concepts in quantum chemical calculations, we refer the reader to ref. 22.

The Volta potential can be obtained by averaging the total electrostatic potential in the direction of the surface normal vector. In the case of a nanotube immersed in water, this corresponds to averaging the electrostatic potential in cylindrical shells around the nanotube center of mass axis, as shown in Figure 1. Given enough vacuum, the average potential reaches an asymptotic value at large distances, which can be taken as the value of the Volta potential. The absolute electrode potential can then be related to experimentally measurable potentials by referencing it to e.g. the standard hydrogen electrode (SHE)

$$U_0^{SHE} = U_0^{abs.} + U_{SHE}^{abs.} \quad (3)$$

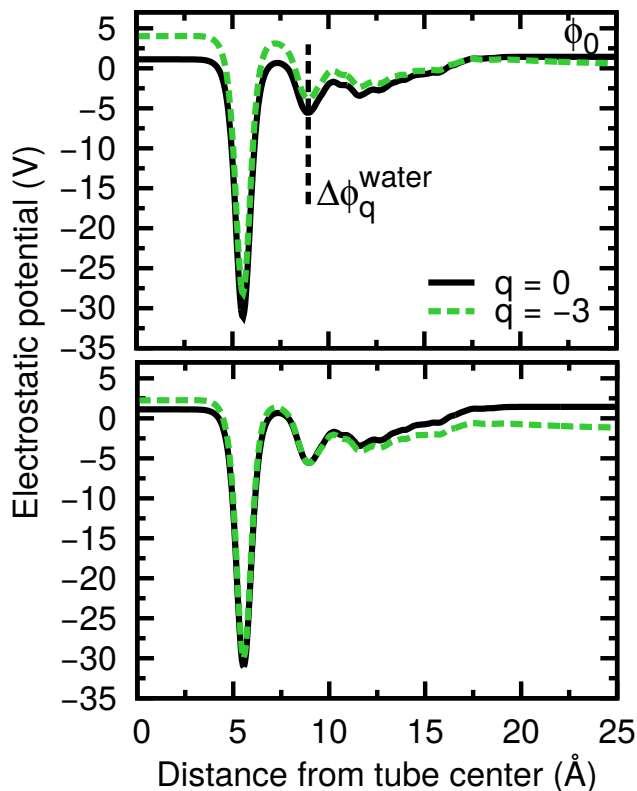


Figure 1. Cylindrically averaged electrostatic potentials for a nanotube immersed in water at different surface charges q (above). Charges are given as multiples of the elementary charge e . Distances greater than 17 Å correspond to the vacuum layer. The neutral system Volta potential ϕ_0 and charge dependent potential alignment term $\Delta\phi_q^{\text{water}}$ are indicated. See main text for the definition of these terms. Below, same as above after the potential alignment term has been added to the $q = -3$ curve.

For the absolute potential of SHE, we use the IUPAC²¹ recommended experimental value of -4.44 V, which is in agreement with the more recent estimate of -4.42 V obtained by Fawcett.²⁴ Nevertheless, several studies^{25–27} have questioned whether this value should be used in quantum chemical calculations, as values differing by several hundred mVs have been reported. An extensive comparison of the various literature values is presented in ref. 28. According to Isse and Gennaro,²⁷ this discrepancy is related to choice of energy zero level and the actual definition of the absolute potential. Indeed, their suggested value of -4.28 V matches Fawcett’s value when the difference in reference points is taken into account. Moreover, it was concluded in ref. 23 that the current computational setup corresponds to the one used to determine the value -4.44 V validating our choice for the potential of SHE. A potentially more serious issue is related to the use GGA

functionals for the Kohn-Sham XC interaction, which, among other issues, leads to an incorrect description of energy levels and band gaps.³ While most GGA functionals typically reproduce accurate vacuum work functions,²² the incorrect alignment of solvent energy levels and the electrode Fermi level might result in unphysical charge transfer between the two combined components.²⁹ For the present system, this matter is addressed in full detail in Sec. 3.1, where we compute the nanotube potential of zero charge using ab initio molecular dynamics.

When the electrode is charged, Eq. 2 is no longer valid due to inclusion of the background charge, preventing the determination of any meaningful Volta potential. To compute the absolute potential of a charged electrode, we reference the charged electrode Fermi level μ_q to the Volta potential of the neutral electrode ϕ_0 , which are calculated at the same atomic configurations. These quantities are, however, not directly comparable because the electrostatic potential of a periodic system has no natural zero point. Traditionally, the total electrostatic potential is referenced to its volume average in the $\mathbf{G} = 0$ cell and set to zero.²⁰ Because the background charge introduces an extra contribution to the total charge density, the electrostatic potential of this system is shifted when compared to the same charge neutral system. Therefore, an additional potential alignment term $\Delta\phi^{water}$ must be included in calculating the absolute potential of charged electrodes

$$U_q^{abs.} = \frac{-\mu_q + e\phi_0}{e} + \Delta\phi_q^{water} \quad (4)$$

Unfortunately, there is no unambiguous way to define the potential alignment term. Following the reasoning of Filhol and Neurock,⁸ we set the reference point at the electrostatic potential minimum corresponding to the first solvation layer, as demonstrated in Figure 1. This choice is motivated by the fact that water and the background charge effectively screen the electric field generated by a charged electrode. Unlike previous studies using the original model, a significant number of explicit water molecules are used throughout this study so that the reference point is always well-defined. This should allow us to compute the electrode potential at low surface charges. An analysis on the sufficiency of the water layer thickness is given in the Supporting Information (SI). In particular, it is shown that for all valid alignment term choices in the present system,

any uncertainty related to computing the electrode potential of charged electrodes cancels when relative energies are considered, see Figure S1. We would nonetheless like to remark that a full quantitative comparison between our potential dependent results and experimental measurements cannot be performed due to a lack of comparable data, even though a qualitative agreement will be established in Secs. 3.2-3.6. On the other hand, these uncertainty factors have no bearing on the investigation of doping effects since the same methodology is consistently applied throughout.

2.2 Construction of Grand Canonical Energies

Once an electrochemical reaction has been modeled at various electrode charges, the potential dependence of the reaction can be derived by comparing calculated absolute energies and potentials in different states of the reaction (e.g. initial and transition state). Prior to this, a twofold correction needs to be applied to the absolute energies E_q of charged systems

$$\Omega = E_q + E_{electron} + E_{size} \quad (5)$$

where Ω is the corrected grand canonical energy, $E_{electron}$ corrects for the varying number of electrons at different charges and E_{size} is a finite-size correction. The first correction term can be interpreted as the work required to remove (add) the excess (missing) electrons from a system where the effective Fermi level is $\mu_0 + \Delta\phi_q^{water}$ ³⁰

$$E_{electron} = q(\mu_0 + \Delta\phi_q^{water}) \quad (6)$$

The effective Fermi level is, to close approximation, equal to the arithmetic mean of the charged and zero charge Fermi levels. The second correction term E_{size} is required to remove the spurious interaction between the actual molecular system and the homogeneous background charge, which results in a slow convergence of the absolute energy with respect to system size. Including this term is vital when studying the formation of charged defects in bulk crystals and several correction methods³¹⁻³⁵ have been proposed with this application in mind. It is worth emphasizing that these

so-called point counter-charge corrections only correct a posteriori the total energy of the system and they do not enter into the electronic structure self-consistency loop. Explicitly removing this interaction would require using, for example, the density³⁶ or local moment³⁷ counter-charge methods.

Contrary to bulk crystal simulations, the electrochemical system under study here is highly anisotropic and it does not fulfill the common assumptions – added charge is localized and uniform dielectric constant – of all the point counter-charge corrections. Indeed, such a correction can only be applied in case the full dielectric tensor of the system is evaluated using computationally demanding density functional perturbation theory.³⁸ Fortunately, as was first noted by Hummer et al.,³⁹ owing to the high polarizability of water, the total energy of a charged, solvated system should converge as a function of the inverse volume of the system; whereas in the absence water, the leading term scales with the inverse cell length. While our system is not fully solvated, finite size tests indicated no discernible difference in energies with growing system size and we subsequently assume this correction term to be negligible. Nonetheless, this methodology leaves room for improvement, as the background charge complicates determining both accurate energies and electrode potentials. In the future, it might be worth considering using explicit counter ions to compensate for the charge of electrode.⁷ Alternatively, a combination of explicit water molecules and a continuum description of the electrochemical double-layer could be employed in the spirit of the modified Poisson-Boltzmann equation approach.^{11–13}

Having corrected the charged system absolute energies, the potential dependence of the grand canonical energies is obtained by fitting a parabola to the graph energy vs absolute potential. This quadratic relationship arises because the combined system of atoms and background charge can be interpreted as a capacitor. For an ideal capacitor, the energy stored in the capacitor depends on potential through

$$\Omega(U) = \frac{1}{2}C(U - U_{pzc})^2 + \Omega_{pzc} \quad (7)$$

where C is the capacitance, U_{pzc} is the potential of zero charge and Ω_{pzc} the corresponding

energy.

2.3 Computational Methods

All reported DFT calculations were performed at the PBE/GGA⁴⁰ level using the spin-dependent formulation of the hybrid Gaussian and plane waves method, as implemented in the open-source CP2K/QUICKSTEP^{41,42} code. To test the accuracy of the PBE exchange-correlation functional, single-point calculations were conducted using the auxiliary density matrix implementation⁴³ of the truncated PBE0⁴⁴ hybrid functional. Van der Waals interactions were included with the DFT-D3 method.⁴⁵ Electrons in the outer most shells of atoms were treated as valence states. The Kohn-Sham orbitals of valence electrons were expanded in molecularly optimized Gaussian basis sets of double- ζ plus polarization quality (MOLOPT-SR-DZVP).⁴⁶ Ionic cores were represented by norm-conserving Goedecker-Teter-Hutter^{47–49} pseudopotentials. The auxiliary plane wave basis set was truncated with a 600 Ry kinetic energy cut off. A similar setup⁵⁰ has recently been demonstrated to yield accurate results for the dissociation of oxygen on doped carbon nanotubes when compared to grid or plane wave implementations of DFT.

The electrochemical hydrogen evolution reaction was studied on a pristine (14,0) carbon nanotube (CNT) C₂₂₄ and on the same nitrogen doped nanotube (NCNT), where a single carbon atom was substituted for nitrogen. The nanotubes were solvated with 331 water molecules (~ 12 Å solvation shell) and a minimum of 15 Å of vacuum separated the periodic copies of the system in directions perpendicular to the nanotube axis, as illustrated in Figure 2. The total system size was $50 \times 50 \times 17.04$ Å³. Both the vacuum layer size and nanotube length were confirmed to be adequate for obtaining converged work functions and absolute energies.

The solvation structure of the NCNT was equilibrated by a 7.5 ps Born-Oppenheimer molecular dynamics simulation in the canonical ensemble at a temperature of 348.15 K. Three linked Nose-Hoover⁵¹ thermostats with a time constant of 200 fs⁻¹ were employed to maintain constant temperature. The ionic cores were propagated using the velocity Verlet algorithm⁵² with a 1 fs time step and deuterium masses for hydrogens. Prior to modeling HER, the solvation structure

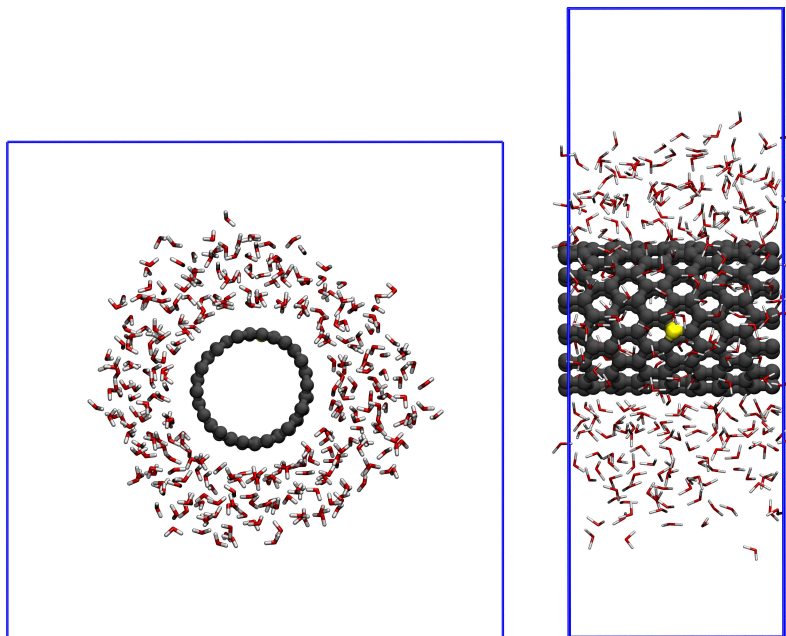


Figure 2. Front (left) and side (right) views of the simulated (14,0) NCNT solvated in water. The snapshots correspond to frame $t = 2$ ps of the molecular dynamics simulation. Carbon atoms are shown in gray, nitrogen in yellow, oxygen in red and hydrogen in white. The periodic boundaries of the system are indicated by the blue wire frame. For clarity, the size of nanotube atoms has been increased.

was fully relaxed by minimizing the force subject to each atom below 0.023 eV/\AA . This water structure was also used for the pristine CNT after an additional relaxation.

The activation energies of each elementary step in HER were determined with the CI-NEB⁵³ method. With the exception of the Tafel reaction, each reaction was modeled at three electrode charges. The reaction paths were represented with 8 (Volmer) or 12 (Tafel/Heyrovsky) images. The charge neutral NEB simulations were considered converged after the maximum force decreased below 0.1 eV/\AA ; tightening the criterion to 0.05 eV/\AA changed activation energies by less than 10 meV. For charged electrodes, a slightly higher 0.13 eV/\AA criterion was employed due to slower convergence of the simulation and no significant changes in reaction path energies during the latter stages of the simulation. The reacting protons were added to water molecules near the surface, which after minimization adopted a Zundel cation H_5O_2^+ formation. All water molecules except the Zundel cation were frozen in the optimized, charge neutral configuration to prevent the electrode potential from shifting due to reorganization of water. To determine the electrode potential in each

NEB image, the electrode Fermi level was calculated by a Fermi-Dirac smearing of the orbital occupations using a 300 K smearing temperature. All energies were extrapolated to zero electronic temperature. An extrapolation method was employed to obtain the grand canonical activation energies on a wider potential scale. Full details of this procedure are reported in Sec. 3.2, while comparisons with unextrapolated results are given in the SI (Figure S4).

3 Results and Discussion

In this section, we begin by assessing the accuracy of the employed computational model for describing the nanotube-water electrochemical interface at charge neutral conditions. In particular, we compute the NCNT potential of zero charge and show that it is in agreement with the experimental estimate. Subsequently, we first consider both the Volmer-Tafel and Volmer-Heyrovsky mechanisms of HER on clean nanotube surfaces, i.e. at a zero surface coverage of hydrogen atoms, with each elementary reaction treated in separate subsections. For the latter mechanism, we also consider the effects of substitutional nitrogen doping and calculate grand canonical activation energies as a function of electrode potential. We conclude by analyzing how the coverage of hydrogens affects HER activation energies for both mechanisms at charge neutral conditions. The results are compared to earlier studies on CNTs, nickel and platinum.

3.1 Evaluating the Accuracy of the Electrochemical Model at Charge Neutral Conditions

For the pristine (14,0) CNT, a vacuum work function of 4.39 eV is obtained using the PBE exchange-correlation functional; while the PBE0 hybrid functional yields a slightly higher value of 4.50 eV. Both of these values match the 4.47 eV estimate that Barone et al.⁵⁴ calculated with the HSE hybrid functional, which has been shown to accurately reproduce the vacuum work function of graphene. The 0.1 eV difference in PBE/PBE0 work functions persists upon introduction of the explicit solvation layer, regardless of the actual orientation of water molecules. All in all, this sug-

gests that an accuracy on the order of 100 mV can be expected for calculated electrode potentials of uncharged nanotubes in static configurations with the computational implementation described in Sec. 2.3. It is worth noting that this difference is significantly smaller than the 0.2 – 0.3 eV difference in HOMO-LUMO band gaps; our calculated band gaps are 0.64 (PBE) and 0.94 eV (PBE0), while 0.85 eV is reported for the HSE functional.⁵⁴ Thus, we find that the relative position of the Fermi level is less sensitive to GGA functional errors than the absolute alignment of electronic levels, in agreement with earlier studies.²²

After a substitutional nitrogen dopant is added to the nanotube, the extra electron from nitrogen is injected to the nanotube conduction band shifting the vacuum PBE work function to 4.15 eV, which is equivalent to a shift of 240 mV in the absolute electrode potential when compared to pristine CNT. This value also quantifies the minimum expected potential shift during an electrochemical reaction, e.g., when a proton is reduced on the nanotube during HER. From an experimental perspective, this shift is unrealistically large and illustrates why constant charge activation energies are not directly comparable to the true constant potential values. In water, the potential shift between pristine and doped CNT is less pronounced remaining below 100 mV for all explored configurations.

A more rigorous test for the accuracy of the present computational setup is the evaluation of the NCNT potential of zero charge U_{pzc} (PZC). As has been previously noted in the study of the Pt(111)-water interface (see e.g. ref. 23 or Table 2 in ref. 22), the PZC is highly sensitive to the orientation of water molecules near the electrode and it is questionable whether reliable estimates can be obtained based on static calculations alone. Here, we calculate the PZC by averaging the electrode potential from a 6.5 ps molecular dynamics simulation following an initial 1 ps equilibration period. To compute the PZC, the electrode potential was sampled every 250 fs, as shown in Figure 3.

According to the figure, the calculated electrode potential fluctuates in a window of roughly 0.5 V in width. From the time averaged potential, we obtain an estimate of -0.19 V vs SHE (0.15 V standard deviation) for the PZC of the studied NCNT. For a mixture of different pristine,

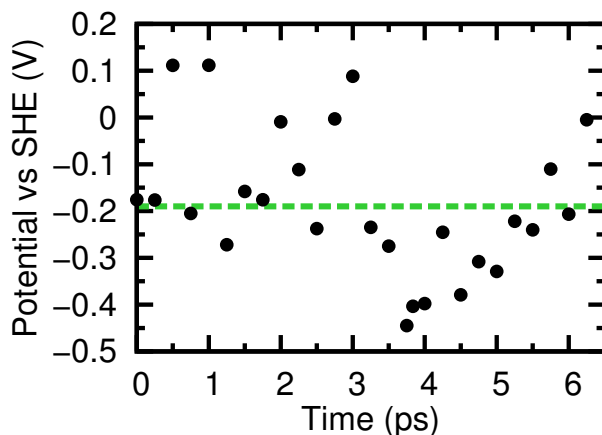


Figure 3. Variation of the NCNT absolute electrode potential during a molecular dynamics simulation. The electrode potential is calculated every 250 fs (dots). The dashed line is an estimate of the potential of zero charge U_{pzc} calculated by averaging all the data points. The time axis zero is set to the first frame after an initial 1 ps equilibration.

single-walled CNTs with diameter in the range 1.2 – 1.4 nm, a PZC of -0.23 V vs SHE (0.0 V vs Ag/AgCl) has been experimentally evaluated by locating the potential with minimum capacitance.⁵⁵ Despite the relatively short simulation time, our calculated value is in excellent qualitative agreement with the experimental result, considering that the single substitutional nitrogen should shift the PZC at most by 100 mV, as discussed above. Comparing the calculated NCNT PZC and the vacuum work function, we find that the work function is shifted, on average, by 0.10 eV ($\Phi_0^{\text{water}} - \Phi_0^{\text{vac}}$) due to presence of water molecules, indicating there is some charge transfer from the electrode to water. However, the magnitude of the charge transfer is not significant, which demonstrates that our nanotube-water interface describes a proper electrochemical system at charge neutral conditions.^{23,29}

The only thing that remains to be characterized is the effect of charging on the electrode potential. A detailed analysis is given in the SI. Here, we conclude that electrode charges between -3 and $+1$ correspond to the electrochemically interesting potential region from -1.5 to $+0.5$ V vs SHE, see Figure S2.

3.2 Volmer Reaction

To determine the most stable surface site for proton electrochemical adsorption, we calculated Gibbs energies of hydrogen adsorption, ΔG_{ads} , to various sites near the nitrogen dopant, shown in Figure S3 of the SI. A full description of the employed methodology and all the computed values are reported in the SI, see in particular Table S1. In summary, these simulations indicate that hydrogen preferentially adsorbs to carbon atoms next to the nitrogen dopant. Out of the three neighboring carbon atoms, the Gibbs energy of adsorption is lowest, 0.25 eV, on site C₁₂₅, which will subsequently be used as the active surface site for the Volmer reaction on NCNT. By contrast, a significantly greater value, 1.15 eV, is obtained for adsorption onto pristine CNT. Furthermore, we find that direct adsorption to nitrogen is unfavorable, $\Delta G_{\text{ads}} = 1.61$ eV, despite a net negative charge on the atom.

Norskøv et al.^{56,57} have demonstrated that the experimentally most active catalysts towards HER exhibit a DFT calculated Gibbs energy of hydrogen adsorption close to 0 eV, giving rise to a volcano shaped curve relating these quantities, as predicted by Sabatier's principle. To first approximation, this observation would suggest an enhanced catalytic activity on the nitrogen doped CNT when compared to the pristine material; while, on the other hand, neither catalyst should approach the activity of platinum ($\Delta G_{\text{ads}} \approx -0.03$ eV⁵⁶). We begin investigating this hypothesis by modeling the first step in HER, namely, the Volmer reaction using the CI-NEB method. For both nanotubes, NEB simulations are conducted with surface charges of $q = 0, -2, -3$. The calculated energy profiles are shown in Figure 4.

An immediate first observation is that the energy profiles for both electrodes are strikingly similar. Indeed, the calculated activation energies for NCNT – 0.52, 0.21 and 0.09 eV (in order of growing surface charge) – and for pristine CNT – 0.54, 0.24 and 0.09 eV – are identical within the 0.1 eV statistical accuracy of GGA level DFT. Importantly, on both nanotubes, activation energies decrease with increasing surface charge, which is a necessary prerequisite for the nanotubes to exhibit a growing Volmer activity when the electrode potential is varied. The reaction energies follow a similar decreasing trend; however, differences between catalysts can also be observed.

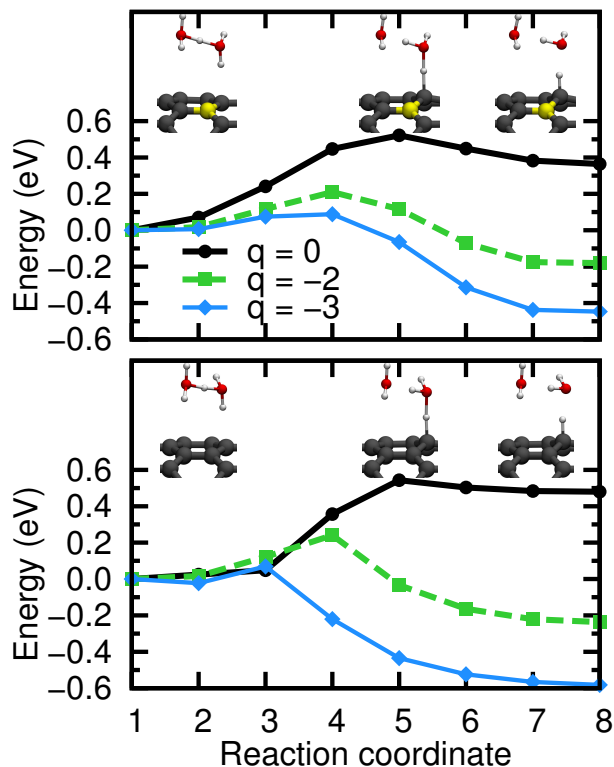


Figure 4. Calculated energy profiles for the Volmer reaction on NCNT (top) and pristine CNT (bottom) with different surface charges q . The lines connecting individual data points are a guide to the eye. The initial, transition and final states (from left to right) of the $q = 0$ reaction are given above the energy profiles. For clarity, only the water molecules participating in the reaction and the surface atoms closest to the active site are shown.

Initially at $q = 0$, the NCNT reaction energy is 0.12 eV lower than the pristine CNT value, but it changes slower with increasing charge and at $q = -3$ the situation is reversed (-0.11 eV). It comes as no surprise that the similarity of the energy profiles is also reflected in the structures of the initial (IS), transition (TS) and final state (FS) of the Volmer reaction, as reported in Tables S2-S3 of the SI. We find that most structural quantities, such as the proton-surface distance in the FS, are insensitive to the surface charge, while others, e.g. the surface-proton distance in the TS, vary systematically with increasing charge for both electrodes.

Our calculated Volmer reaction activation energies are slightly lower than the values $-1.2, 1.0, 0.4$ eV at equivalent charges of $q = 0, -1.4, -4.2$ (normalized by the number of nanotube atoms) – reported by Das et al.¹⁷ in a recent study of HER on pristine (10,10) CNTs and CNT bundles. Additionally, we observe no doping effect, whereas Deng et al.¹⁸ note that substitutional nitrogen

doping of an iron nanoparticle encapsulated (6,6) CNT lowers the Volmer reaction activation energy from 1.20 to 0.85 eV at charge neutral conditions (for comparison, the authors report a 2.2 eV barrier for the pristine CNT). These discrepancies are most likely explained by differences in computational setups, e.g., the tube chirality and treatment of water molecules. To investigate how sensitive the results are to the XC functional, we recomputed both activation and reaction energies with the PBE0 hybrid functional at the PBE optimized atomic configurations. Compared to PBE values, PBE0 activation energies are approximately 0.1 eV higher and reaction energies 0.1 eV lower at $q = 0$, which is consistent with the Hartree-Fock term increasing charge localization. Additionally, we find both quantities decrease slower as a function of surface charge with the PBE0 functional.

Next, we use the calculated, constant charge activation energies from Figure 4 to construct potential dependent grand canonical activation energies. As mentioned in Sec. 2.3, we use an approximate extrapolation method to compute activation energies at surface charges that have not explicitly been modeled with NEB. In practice, for instance, the converged IS and TS structures from the charge neutral simulation were directly used to compute the absolute energies of the corresponding states at charge $q = +1$. This approximation rests on the assumption that the structures of different reaction states vary smoothly with surface charge. For the Volmer reaction, this clearly is the case as was discussed above. Furthermore, since the calculated energies are insensitive to slight variations in bond lengths, the expected error from the extrapolation procedure is small. While this procedure leaves room for improvement, neglecting it results in minor differences (< 0.2 eV) in calculated activation energies at the extremes of the electrode potential window, see the comparison in Figure S4 of the SI. We wish to emphasize that both methods for computing grand canonical barriers yield a consistent, quantitative overview of the reaction's potential dependence. By contrast, if canonical activation energies are directly used to determine this dependence (see Figure S4), significant deviations from the constant potential behavior are observed. This clearly illustrates the need to include the effects of changing electrode potential when studying electrochemical surface reactions.

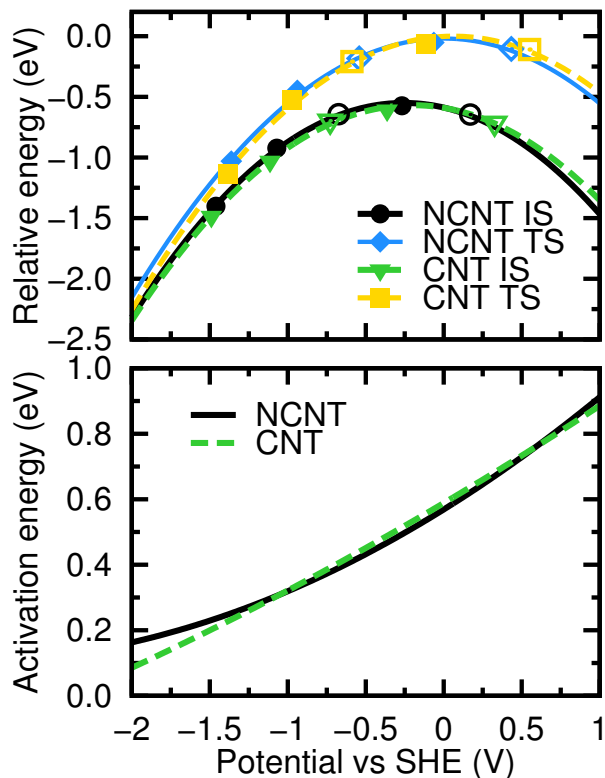


Figure 5. Absolute energies of the Volmer reaction IS and TS as a function of electrode potential for NCNT and pristine CNT (top). Solid points are values from NEB simulations (Figure 4), unfilled points have been calculated using the extrapolation method detailed in the main text. Below, potential dependent grand canonical activation energies determined by fitting parabolas to the TS and IS energies and subtracting the curves. Coefficients of determination $R^2 = 0.998, 0.995, 0.998, 0.993$ in legend order.

The absolute energies of the Volmer reaction IS and TS are plotted against electrode potential in Figure 5. The absolute energies at different charges were corrected according to Eq. 5. By fitting parabolas to the energies, we obtain potential dependent grand canonical activation energies by subtracting the TS and IS parabolas, as illustrated in the same figure. The excellent coefficients of determination serve as a further validation of the extrapolation method employed. For both catalysts, activation energy depends strongly on potential decreasing from 0.57 eV at the thermodynamic redox potential of hydrogen, $U = 0$ V vs SHE, to ~ 0.13 eV at $U = -2$ V. It is worth noting that the computational potential scale is technically not bounded because the stability region of DFT water has not been established. In particular because no actual counter-electrode is present, unphysical reactions, such as the decomposition of water via the alkaline HER reaction

($2\text{H}_2\text{O} + 2\text{e}^- \rightarrow \text{H}_2 + 2\text{OH}^-$), are also possible, although in reality the preceding reaction would require neutral or basic conditions due to the compensating half reaction at the counter-electrode. In accordance with the constant charge activation energies, no statistically significant difference between nitrogen doped and pristine CNTs is observed in the potential dependent energies. The same conclusion holds if we compare potential dependent reaction energies between $U = -1$ V and $U = 0$ V, see Figure S6 of the SI. To put the calculated values into perspective, they should be compared to the computational activation energy on Pt(111), which is slightly higher 0.69 eV at $U = 0$ V but decreases faster with increasing negative potential (0.44 eV/V vs ~ 0.25 eV/V).¹⁵ Despite the seemingly improved Volmer reaction activity at low overpotentials, it turns out the formation of molecular hydrogen is the rate-determining step in HER and a more relevant comparison between the catalysts will be given in Sec. 3.4.

Before concluding this section, we consider the electrochemical adsorption of a second proton onto a surface site next to the site with an already bound hydrogen. This reaction is, of course, necessary for the formation molecular hydrogen through the Tafel mechanism. The methodology used to characterize this reaction is identical to the first one; however, here, we only consider the reaction on the nitrogen doped CNT. This choice was primarily motivated by the fact that the Tafel reaction turns out to be energetically unfavored for the studied nanotubes, as will be shown in Secs. 3.3 and 3.6. The calculated NEB energy profiles and the potential dependence of the reaction grand canonical activation energy are plotted in Figure S5 of the SI. Both figures indicate that adsorbed hydrogen increases the reactivity of neighboring surface sites for further reactions. Altogether, a 0.15 eV decrease in grand canonical activation energies is observed over the potential range $U = -2$ V to $U = 0$ V.

3.3 Tafel Reaction

Next, we model the formation molecular hydrogen through the Tafel mechanism. Here, we have assumed that the reacting hydrogen atoms are bonded to neighboring surface atoms in the initial state although other sites in the carbon hexagon could also be utilized. Because the Tafel reaction

is a Langmuir-Hinshelwood type surface reaction, the reaction should be mostly independent of the solvation environment. Consequently, to prevent water molecules from participating in the reaction, we allowed the hydrogen molecule to form a cavity in the solvent structure near the active surface sites and froze all water molecules in this configuration. The calculated minimum energy path on the NCNT electrode is shown in Figure 6 at zero surface charge. The NEB calculation was not fully converged (max force ~ 0.36 eV/Å), as below we demonstrate that the reaction mechanism is chemically unrealistic on the surface sites in question.

From the calculated energy profile, we find a 2.4 eV energy barrier for the Tafel reaction, which is significantly larger than the corresponding value for the Volmer reaction. While this barrier is in agreement with earlier studies,^{17,18,58} analysis of the reaction mechanism reveals it is unlikely that hydrogen atoms bound to adjacent surface sites react through this mechanism, see top panel of Figure 6. The atoms do not react directly on top of the carbon-carbon bond. Instead, we find that the hydrogen initially farther away from the nitrogen dopant first desorbs and then reacts with the second atom. In the transition state, the hydrogen atom is located at height of 2.3 Å as measured from the surface. This distance is only 0.6 Å shorter than the average carbon-oxygen distance of the first solvation shell determined from the ab initio molecular dynamics simulation. Indeed, if the hydrogen molecule was not allowed to form a cavity in the water structure near the surface, the desorbed hydrogen atom would bind to water oxygen. The reaction would then proceed through the Heyrovsky mechanism and with a decidedly lower activation energy, see Sec. 3.4.

The unfavored Tafel reaction between atoms located on adjacent surface sites can be understood by a simple molecular orbital analysis. Because the hydrogen molecule antibonding σ^* orbital is located at the “ends” of the molecule, the overlap between the hydrogen σ^* and nanotube π orbitals is maximal when the atoms react directly on top of the carbon-carbon bond favoring dissociation. To minimize orbital overlap, one of the atoms desorbs prior to reacting, which leads to a lower activation energy but an unrealistic mechanism. It is worth emphasizing that the Tafel reaction is by no means impossible on CNTs, as hydrogen atoms bound to other sites,⁵⁸ adjacent nanotubes,¹⁷ structural defects, or a finite coverage of adsorbed hydrogen atoms might facilitate the reaction.

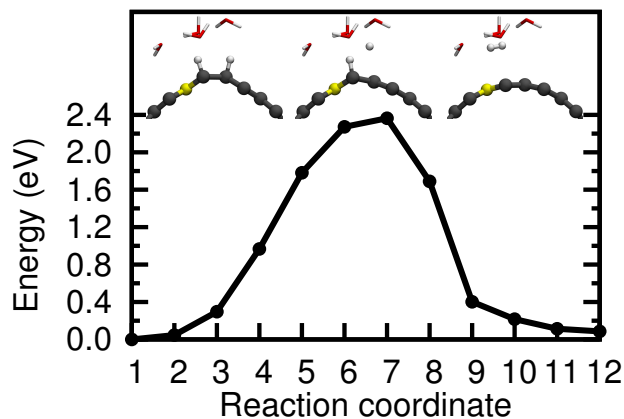


Figure 6. Calculated energy profile for the Tafel reaction on a charge neutral NCNT. The labels of Figure 4 apply to this figure. As described in the main text, the simulation was not fully converged.

This matter will be further discussed in Sec. 3.6 where we investigate hydrogen coverage effects.

3.4 Heyrovsky Reaction

On both nanotubes, Heyrovsky reaction minimum energy paths were determined at surface charges $q = 0, -1, -2$ and are shown in Figure 7. Irrespective of nanotube charge, we find that the activation energy of the Heyrovsky reaction is significantly lower than that of the Tafel reaction. This clearly verifies our earlier assumption that the Volmer-Heyrovsky path should be the predominant HER mechanism on clean CNTs. Quite unexpectedly, the energy profiles indicate that the activation energies on the pristine CNT – 1.09, 0.91, 0.78 eV – are lower than the corresponding values 1.33, 1.15, 1.02 eV on NCNT. The pristine CNT activation energies are in excellent agreement with earlier results.¹⁷ A similar trend is observed for reaction energies which are approximately 0.4 eV lower on pristine CNT. It is worth noting that the simulations of Deng and co-workers¹⁸ also indicate a 0.24 eV increase in Heyrovsky barriers due to nitrogen doping of a Fe encapsulated CNT (1.26 eV barrier with nitrogen, 1.02 eV without), despite showing an opposite effect for the Volmer reaction (see discussion in Sec. 3.2). In contrast to experimental data, which indicate a 200 mV decrease in onset potential due to nitrogen doping,^{18,59} our observations suggest that substitutional nitrogen doping of CNTs decreases the material’s electrocatalytic activity towards HER seeing as there were only minor differences in the reaction energies of the first HER step. To investigate the

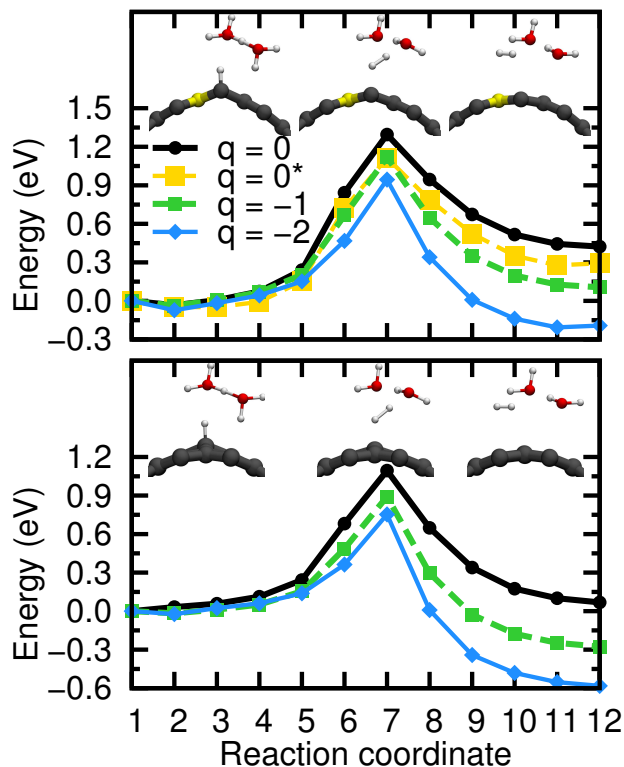


Figure 7. Calculated energy profiles for the Heyrovsky reaction on NCNT (top) and pristine CNT (bottom) with different surface charges q . The curve marked with an asterisk has been obtained using a different initial location for the reacting Zundel cation, see the main text. Note the difference in energy axis scales.

matter further, we recomputed the $q = 0$ energy profile on the NCNT by changing the initial location of the reacting Zundel cation from above a carbon atom adjacent to the Volmer reaction active site (site C₆₆) to directly above the nitrogen dopant (site N₇₀). The resulting minimum energy profile is shown in Figure 7 together with the other calculated profiles.

From the figure, it is seen that changing the initial location of the Zundel cation lowers the Heyrovsky reaction activation energy from 1.33 to 1.16 eV. The latter value, although slightly higher, matches the pristine CNT barrier of 1.09 eV within the 0.1 eV error margin. Similarly, we find that the reaction energy also decreases by 0.13 eV. The 0.17 eV reduction in barrier height can be mostly attributed to an energetically less stable initial configuration. Indeed, as virtually no reduction in the reverse barrier is observed, it is evident that there is little charge transfer from the nitrogen dopant to the forming hydrogen molecule because this would lower the energy of the

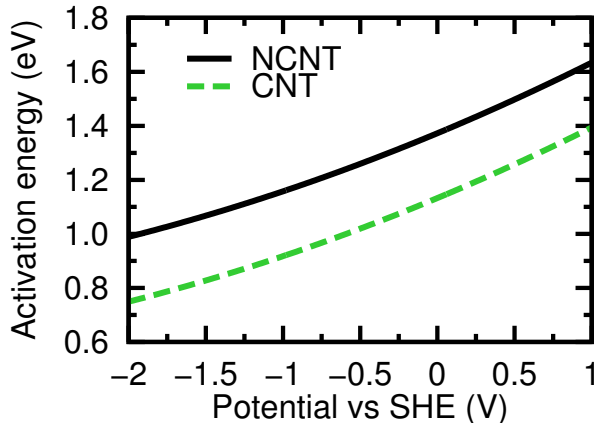


Figure 8. Potential dependent grand canonical activation energies for the Heyrovsky reaction on pristine and nitrogen doped CNTs.

TS relative to the final state. Overall the effect of substitutional nitrogen seems localized only to nearest neighbors manifesting as higher C – H bond energies, in line with the observations in Sec. 3.2. Given that in solution at ambient temperature all possible approach directions for the Zundel cation should be equally likely, we expect the effective activation energy on the NCNT to be roughly equal to, or at maximum 0.1 eV higher than on pristine CNT. However, this matter cannot be completely settled without further calculations.

As before, the calculated activation energies of Figure 7 were used to determine the potential dependence of the Heyrovsky reaction grand canonical activation energy, illustrated in Figure 8. The corresponding reaction energies are given in Figure S6 of the SI. On pristine CNT, the Heyrovsky reaction barrier is around 1.13 eV at $U = 0$ V and decreases quite linearly with a 0.15 eV/V slope when going towards negative potentials. For NCNT, a similar shaped curve is obtained but it is shifted upwards in the energy axis by 0.2 eV. The unrealistically large shift is a direct consequence of using the values from Figure 7 as we did not repeat the charged nanotube calculations with the different initial position of the Zundel cation, see the discussion above.

3.5 Standard Free Energy Diagram

To discuss the energetics of the entire hydrogen evolution reaction on the studied CNTs, we use the calculated potential dependent activation energies from Figures 5 and 8, and the reaction ener-

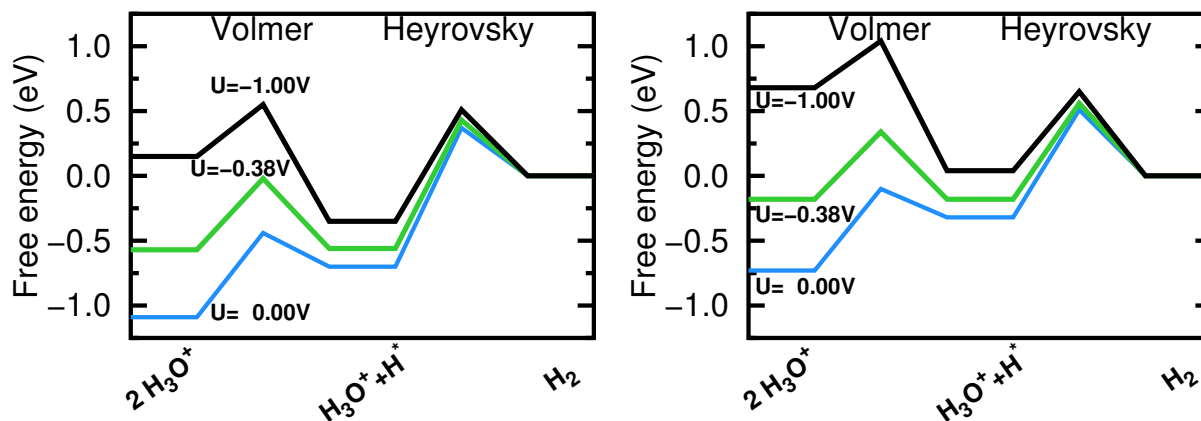


Figure 9. Standard free energy diagrams for HER proceeding through the Volmer-Heyrovsky mechanism on NCNT (left) and CNT (right) at selected electrode potentials.

gies from Figure S6 in the SI to construct standard free energy diagrams for the Volmer-Heyrovsky mechanism. These diagrams are shown for different electrode potentials in Figure 9. A full account of the methodology for obtaining free energies as well as the employed thermodynamic information is given in the SI. Here, the comparison between NCNT and CNT is insensitive to whether we consider energies or standard free energies, see Figure S7 for comparison.

From Figure 9, it is evident that the energetics of the Volmer step are virtually identical on both CNT and NCNT. This step becomes exergonic, $\Delta G < 0$, at $U = -0.38\text{ V}$. Regardless of potential, the effective barrier of HER is determined by the formation of molecular hydrogen through the Heyrovsky reaction, whose activation free energy is at least 0.2 eV greater than the Volmer step on pristine CNT (0.6 eV greater activation energy). Assuming similar kinetic factors, the Heyrovsky reaction should therefore be the rate-limiting step of HER on carbon nanotubes, which is consistent with experimental Tafel slope analysis on a variety of functionalized single-walled CNTs.^{18,60,61} The free energy diagrams indicate that pristine CNT is more active than NCNT due to more favorable Heyrovsky step energetics; however, we again wish to emphasize that a portion of this difference is an artifact as was explained in Sec. 3.4.

Skúlason et al.¹⁵ have calculated the activation energy of the Tafel reaction on Pt(111) – the rate-determining step of HER on platinum – at several electrode potentials. According to their results, the reaction barrier is approximately 0.8 eV at $U = 0\text{ V}$ and begins rapidly decreasing to-

wards zero at $U = -0.25$ V. Comparing the rate-determining step barriers, we find that the studied CNT is less active towards HER than Pt owing to the 0.3 eV larger activation energy at $U = 0$ V, given the similarities in computational setups. This conclusion is in agreement with experimental results, which indicate a significantly lower HER onset potential on Pt, see e.g. ref. 18.

Strictly speaking, the energy diagrams of Figure 9 are valid only at a zero surface coverage of hydrogen atoms, θ , since we have assumed that there are no additional hydrogens near the reaction active site. This approximation is poor at potentials greater than the onset potential of HER. Indeed, if we estimate the surface coverage using the computed Volmer reaction energies and a simple, non-interacting Langmuir model, the analysis reveals that the coverage is already 0.48 monolayer at $U = -0.38$ V and reaches unity at $U = -0.5$ V under ambient conditions, see Figure S8. In the next section, we will explore how coverage effects influence the energetics of each elementary step in HER. Before concluding this section, we estimate the computational HER onset potential by neglecting the dependence of activation energy on coverage, which is a valid approximation for potentials below the onset potential as the coverage is still low, see Figure S8.

Assuming a proton concentration of $c_{\text{H}^+} = 1$ M (i.e. pH = 0) and a rate-determining Heyrovsky step, the Volmer-Heyrovsky rate is given in units of current density (A cm^{-2}) by

$$i = -\frac{e\nu N\theta(U)}{A} \exp\left(-\frac{G_a^{\text{Heyrovsky}}(U)}{k_B T}\right) \quad (8)$$

where $\nu = 10^{13} \text{ site}^{-1}\text{s}^{-1}$ is the approximate attempt frequency,⁶² N is the number of surface sites, A is the geometric surface area and $G_a^{\text{Heyrovsky}}(U)$ is the Heyrovsky activation free energy. With this kinetic model, we obtain a HER onset potential of approximately $U = -0.34$ V for both nanotubes as illustrated in Figure S8, employing a typical 2.6 w-% nitrogen doping concentration. Despite the (slightly unrealistic) difference in Heyrovsky step energetics on NCNT and CNT, this has no observable effect on the rate of HER. All in all, our results suggest that the single substitutional nitrogen doping does not alter the HER activity of CNTs at potentials below the onset potential of HER, where coverage effects can safely be neglected ($\theta = 0.16$ at $U = -0.34$ V, but $\theta = 0.04$ at $U = -0.3$ V). The calculated onset potential is in fair agreement with the experi-

mental range of potentials $-(0.4 - 0.5)$ V reported for pristine single- and multi-walled CNTs in acidic conditions.^{18,60,61} Additionally, this observation matches the findings of Taylor et al.,¹⁶ who studied Ni(111) at ambient conditions and demonstrated an excellent correspondence between experimental and computational onset potentials by considering Volmer-Heyrovsky reaction free energies, computed using a similar potential controlling method in conjunction with thermodynamic Born-Haber cycles.

3.6 Effects of Hydrogen Coverage

To explore the effects of hydrogen coverage, we have first computed hydrogen adsorption energies onto the active surface site in HER for a variety of different hydrogen configurations near the active site. The full set of values for both NCNT and CNT are given in the SI, Tables S7-S8. By comparing these values to the corresponding adsorption energies on the clean nanotubes, two main features can be distinguished. Firstly, the adsorption process becomes increasingly exothermic when surface sites directly next to the active site are occupied, consistent with results presented in the SI for the Volmer reaction of a second proton (see also Sec. 3.2). Secondly, any occupied site two bonds distant has an opposite effect on the adsorption energy. As the number of occupied sites one and two bonds distant are varied, a wide range of adsorption energies are observed. Surprisingly, this range is similar for both nanotubes even though the magnitude of change in adsorption energies is very different for the explored configurations (the sign is the same in each case).

By virtue of the Brønsted-Evans-Polanyi (BEP) relationship,¹⁵ configurations with more endothermic hydrogen adsorption energies should be more reactive towards the Heyrovsky and Tafel reactions than the clean nanotubes, because an increase in adsorption energy translates into a weaker C – H bond. The converse should hold for the Volmer reaction. This analysis illustrates that on CNTs at fixed electrode potential the HER reactivity of a site should be dependent on the distribution of adsorbed hydrogen atoms around the site, whereas the probability of observing a given distribution depends on coverage and the interaction between sites. While it is in principle

possible to extract the average number of neighboring hydrogens (as a function of distance) using an interacting lattice Monte Carlo model, this is beyond the scope of the current study. Instead, to gain insight into the relationship between activity and the distribution of adsorbed hydrogens, we repeated the charge neutral NCNT Volmer and Heyrovsky NEB calculations for two hydrogen configurations; one with a more endothermic 1.04 eV adsorption energy, and one with a more exothermic -0.58 eV adsorption energy (see Table S7). For comparison, we also used these same configurations for pristine CNT, although the latter configuration has nearly an identical adsorption energy in comparison to the clean surface (see Table S8). The calculated activation energies including the data from Figure 7 are shown with respect to adsorption energy in Figure 10.

Despite the worse linear fits for CNT, we find that the activation energies for both reactions fol-

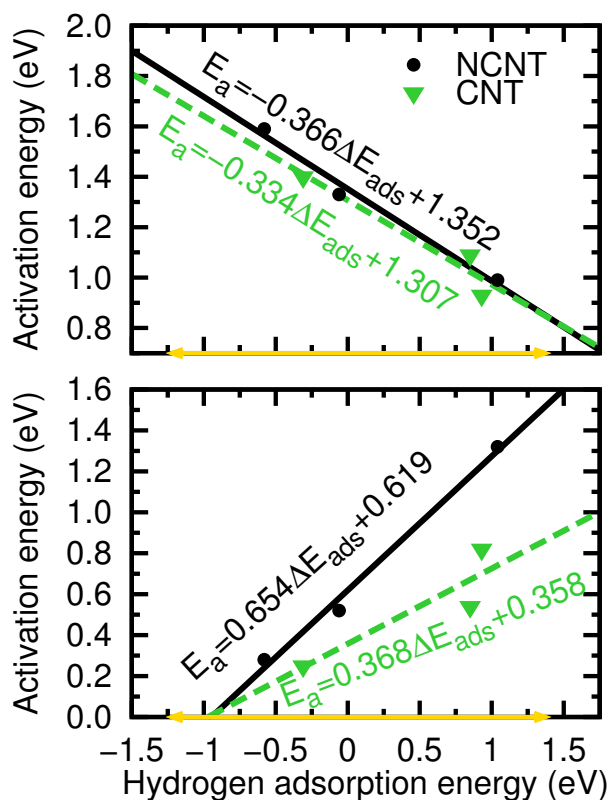


Figure 10. Calculated Heyrovsky (top) and Volmer (bottom) activation energies on NCNT and CNT as a function of hydrogen adsorption energy, measured for adsorption onto the active surface site. Different activation energies correspond to a distinct distribution of adsorbed hydrogen atoms near the active site (points). The lines are linear fits to the individual data points with equations indicated. The range of observed adsorption energies on NCNT is shown by the yellow arrow. $R^2 = 0.983, 0.918, 0.991, 0.802$ (top-to-bottom order).

low a BEP relationship, i.e., Heyrovsky reaction activation energies decrease linearly with growing adsorption energy, whereas the Volmer barriers show a reverse linear dependence. An analogous relationship between adsorption and reaction energies can also be deduced, see Figure S9. Comparing the Heyrovsky barriers on NCNT and pristine CNT, no difference between the two electrodes is observed assuming the standard 0.1 eV error margin. Interestingly, the 0.24 eV higher barrier on clean NCNT, which was discussed in Sec. 3.4, is fully negated by the difference in adsorption energies on CNT and NCNT. On the contrary, the Volmer barriers exhibit a clear difference between the catalysts, since for NCNT the barrier grows approximately 1.8 times faster with increasing adsorption energy. The Volmer barriers of Figure 10 are by construction upper bounds because we only consider reactions where the proton binds to the active site at a fixed distribution of adsorbed hydrogens near the site; while other orders of filling the sites might lead to an overall lower Volmer barrier based on the adsorption energy calculations.

By the previous analysis, hydrogen configurations that destabilize the C – H bond should also lower the activation energy for the Tafel reaction. Consequently, we repeated the Tafel reaction of Sec. 3.3 for a configuration where two of the four second nearest neighbor sites of both active sites were occupied by hydrogen atoms, corresponding to a 0.69 eV adsorption energy (see Table S7). These calculations were not performed on CNT as we observed no difference between NCNT and pristine CNT for the Heyrovsky reaction. As expected, we find that this procedure lowers the Tafel barrier from ~ 2.4 eV to 1.8 eV. However, noting that the adsorption energy for a configuration where all the second nearest neighbors are occupied, which we expect to be the most endothermic configuration for the Tafel reaction, is only 0.09 eV more endothermic, the reaction barrier is expected to be too large for all possible hydrogen configurations in order for the Tafel reaction to be catalytically relevant. Moreover, if we use the linear relationship from Figure 10 to calculate the Heyrovsky barriers for the simulated hydrogen configurations, the Heyrovsky barriers are 1.0 and 0.7 eV lower than the respective Tafel values. Clearly, this indicates that the Volmer-Heyrovsky mechanism is the primary HER mechanism for the investigated sites and should account for most of the electrocatalytic activity. Exploiting the fact that experimentally HER follows the Volmer-

Heyrovsky path on both Ni(111) and pristine CNTs, the same conclusion should be valid for any potential between $U = -2$ V and $U = 0$ V, since on nickel the Tafel reaction becomes increasingly endothermic, i.e. the barrier rises, when going towards more anodic potentials.¹⁶

As demonstrated in Sec. 3.5, the nanotube hydrogen coverage rapidly approaches full monolayer once the electrode potential increases beyond the HER onset potential $U = -0.34$ V. We can use the calculated BEP relationships from Figures 10 and S9 to estimate how the energetics of the Volmer-Heyrovsky mechanism change in the limit of monolayer coverage. To facilitate comparison between NCNT and CNT, the following scheme is used to compute hydrogen adsorption energies onto the active site at full monolayer coverage. On NCNT, it is calculated as the average energy for adsorption onto the three carbon sites next to the unoccupied nitrogen dopant with all remaining carbon sites occupied. The same definition is employed for pristine CNT but the nitrogen is replaced by an occupied carbon atom.

This procedure yields adsorption energies of -1.00 and -0.67 eV for CNT and NCNT, respectively. With these values, we obtain the Volmer-Heyrovsky energy diagrams shown in Figure 11. For comparison, data for zero hydrogen coverage is also included, as computed from the NEB

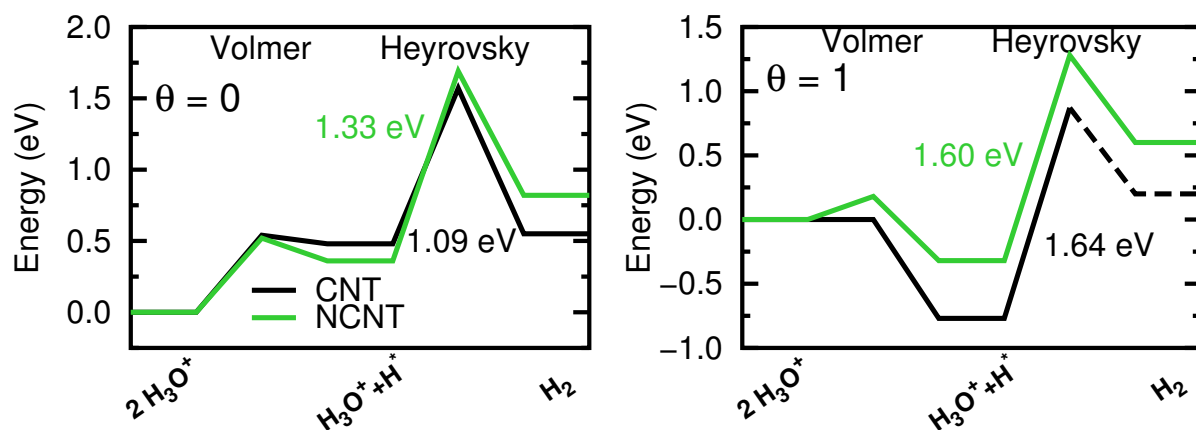


Figure 11. Energy profiles for the Volmer-Heyrovsky reaction on CNT and NCNT at hydrogen coverages of $\theta = 0$ (left) and $\theta = 1$ (right). Data for $\theta = 0$ is from Figures 4 and 7, while for $\theta = 1$ it is calculated using the fitted BEP relationships from Figures 10 and S9. Maximum barriers along reaction path are indicated. The energy reference is set to the reaction initial state, because an accurate value for the Heyrovsky reaction energy on CNT at $\theta = 1$ cannot be determined due to a poor fit (dashed portion).

simulations of Figures 4 and 7. Regardless of coverage, we find that the barrier for the Heyrovsky step is larger than for the Volmer step, thus reinforcing our earlier conclusion that this step should determine the rate of HER. The 0.24 eV difference between Heyrovsky barriers on clean CNT and NCNT surfaces vanishes at full monolayer coverage, and in this limit the NCNT barrier is in fact 0.04 eV lower. This a key discovery since it illustrates that the nanotubes become more alike as coverage increases. Here, the actual barriers are not relevant because they are valid for charge neutral nanotubes which are outside the potential range where monolayer hydrogen coverage is possible.

The present analysis suggests that while we are unable to comment on how the absolute energetics of the Volmer-Heyrovsky mechanism change at high electrode potentials when coverage effects are included, the relative difference between NCNT and CNT in Figure 9 should be less pronounced, especially if effects of Zundel cation approach direction were also considered. On the other hand, none of the results indicate that this change would be so profound that the activity of NCNT would exceed that of pristine CNT. Our coverage dependent analysis is of course an oversimplification because we have assumed the surface sites to be non-interacting, whereas a larger number of active sites would need to be investigated to derive a precise microkinetic model for HER. Nonetheless, because there was no difference at low potentials and zero coverage either, our results demonstrate that single, substitutional nitrogen doping has no observable effect on computational HER activity, at least when focusing on a site directly next to the nitrogen dopant which based on the clean surface adsorption energies should be the most active towards HER. Given that the hydrogen adsorption (free) energy is much lower on NCNT than on CNT, this observation seems to contradict the proposed volcano plot⁵⁶ relating experimental HER activity with DFT hydrogen adsorption energies. Judging by the maximum activation energies along the Volmer-Heyrovsky path, no improvement due to nitrogen doping was actually observed for Fe encapsulated CNTs (1.26 eV barrier with nitrogen, 1.20 eV without), despite a similar difference in adsorption energies.¹⁸ Naturally, if we associate the calculated adsorption energies with experimental HER activities, the results will match the predictions of the volcano plot; but since

the exact, atomic-level structure of experimental NCNTs is unknown and usually contains nitrogen in various bonding configurations,⁶³ we do not believe this comparison to be fully relevant. In conclusion, our computational results do not support the claim that the enhanced HER activity on NCNTs is due to lone substitutional nitrogen atoms. Further research is however required to assess whether different nitrogen configurations or tube chiralities could explain the experimental decrease in onset potential.⁵⁰

4 Conclusions

The electrochemical hydrogen evolution reaction was investigated in acidic solution on pristine and nitrogen doped carbon nanotubes using density functional theory. By calculating the activation and reaction energies of each elementary step in HER (the Volmer, Tafel and Heyrovsky reactions), it was concluded that the Volmer-Heyrovsky mechanism should be the predominant HER reaction mechanism on carbon nanotubes in agreement with experimental measurements. Furthermore, we found that the Heyrovsky reaction is the rate-determining step owing to its larger energy barrier. Substitutional nitrogen doping of the nanotube did not improve the material's electrocatalytic activity towards HER. In light of experimental evidence that indicate an enhanced activity on nitrogen doped CNTs, further research is required to quantify which nitrogen configurations contribute to HER activity.⁵⁰

In experimental electrochemistry, the catalytic activity of a prospective catalyst material is measured as a function of electrode potential. To obtain comparable results, we repeated barrier calculations for the Volmer-Heyrovsky mechanism at different nanotube charges, allowing us to determine constant potential (grand canonical) activation energies on a continuous electrode potential scale. This procedure was shown to be necessary for obtaining a reliable description of the reaction's potential dependence; although, we were unable to fully assess the quantitative accuracy of the potential dependent barriers due to a lack of comparable experimental data, while qualitative agreement was readily established. Based on computed potential dependent activation

energies, both nanotubes exhibited electrocatalytic activity towards HER, seen as a decrease in the barriers with increasing potential. We report an effective activation energy of 1.13 eV for HER on pristine CNT at $U = 0$ V, where the effects of hydrogen coverage can safely be omitted. Compared to platinum, the barrier of the rate-determining step is substantially larger, explaining the superior activity of Pt observed in experiments.

To investigate how a non-zero hydrogen coverage influences the energetics of HER, we established a linear relationship between activation energies and the distribution of hydrogen atoms near the active surface site using vacuum adsorption energies as the descriptive variable. This analysis demonstrated that the reaction is sensitive to the conditions at the nanotube surface, but that no difference between NCNT and CNT is observed at the limit of full monolayer coverage. Additional simulations are however necessary to accurately determine the average coverage and distribution of adsorbed hydrogens and to relate these quantities to the applied electrode potential, which would then facilitate the development of a complete computational model of HER on CNTs.

Acknowledgement

This study was financed by the Academy of Finland through its Centres of Excellence Program, project no. 251748. NH acknowledges financial support from Aalto University School of Chemical Technology in the form of a PhD scholarship. Computational resources were provided by CSC – the Finnish IT Centre for Science and the Swiss National Supercomputing Centre (CSCS).

Supporting Information Available

Additional discussion regarding the computational methodology; Figures S1-S9; Tables S1-S8. This material is available free of charge via the Internet at <http://pubs.acs.org>.

References

- (1) Nørskov, J. K.; Abild-Pedersen, F.; Studt, F.; Bligaard, T. Density Functional Theory in Surface Chemistry and Catalysis. *Proc. Natl. Acad. Sci. U.S.A.* **2011**, *108*, 937–943.
- (2) Carloni, P.; Rothlisberger, U.; Parrinello, M. The Role and Perspective of Ab Initio Molecular Dynamics in the Study of Biological Systems. *Acc. Chem. Res.* **2002**, *35*, 455–464.
- (3) Cohen, A. J.; Mori-Sánchez, P.; Yang, W. Challenges for Density Functional Theory. *Chem. Rev.* **2011**, *112*, 289–320.
- (4) Kaduk, B.; Kowalczyk, T.; Van Voorhis, T. Constrained Density Functional Theory. *Chem. Rev.* **2012**, *112*, 321–370.
- (5) Alavi, A.; Kohanoff, J.; Parrinello, M.; Frenkel, D. Ab Initio Molecular Dynamics with Excited Electrons. *Phys. Rev. Lett.* **1994**, *73*, 2599–2602.
- (6) Lozovoi, A. Y.; Alavi, A.; Kohanoff, J.; Lynden-Bell, R. M. Ab Initio Simulation of Charged Slabs at Constant Chemical Potential. *J. Chem. Phys.* **2001**, *115*, 1661–1669.
- (7) Rossmeisl, J.; Skúlason, E.; Björketun, M. E.; Tripkovic, V.; Nørskov, J. K. Modeling the Electrified Solid–Liquid Interface. *Chem. Phys. Lett.* **2008**, *466*, 68–71.
- (8) Filhol, J.-S.; Neurock, M. Elucidation of the Electrochemical Activation of Water over Pd by First Principles. *Angew. Chem. Int. Ed.* **2006**, *45*, 402–406.
- (9) Taylor, C. D.; Wasileski, S. A.; Filhol, J.-S.; Neurock, M. First Principles Reaction Modeling of the Electrochemical Interface: Consideration and Calculation of a Tunable Surface Potential from Atomic and Electronic Structure. *Phys. Rev. B* **2006**, *73*, 165402.
- (10) Otani, M.; Sugino, O. First-Principles Calculations of Charged Surfaces and Interfaces: A Plane-Wave Nonrepeated Slab Approach. *Phys. Rev. B* **2006**, *73*, 115407.

- (11) Jinnouchi, R.; Anderson, A. B. Electronic Structure Calculations of Liquid-Solid Interfaces: Combination of Density Functional Theory and Modified Poisson-Boltzmann Theory. *Phys. Rev. B* **2008**, *77*, 245417.
- (12) Fang, Y.-H.; Liu, Z.-P. Mechanism and Tafel Lines of Electro-Oxidation of Water to Oxygen on RuO₂(110). *J. Am. Chem. Soc.* **2010**, *132*, 18214–18222.
- (13) Letchworth-Weaver, K.; Arias, T. A. Joint Density Functional Theory of the Electrode-Electrolyte Interface: Application to Fixed Electrode Potentials, Interfacial Capacitances, and Potentials of Zero Charge. *Phys. Rev. B* **2012**, *86*, 075140.
- (14) Nielsen, M.; Björketun, M. E.; Hansen, M. H.; Rossmeisl, J. Towards First Principles Modeling of Electrochemical Electrode–Electrolyte Interfaces. *Surf. Sci.* **2015**, *631*, 2–7.
- (15) Skúlason, E.; Tripkovic, V.; Björketun, M. E.; Gudmundsdóttir, S.; Karlberg, G.; Rossmeisl, J.; Bligaard, T.; Jónsson, H.; Nørskov, J. K. Modeling the Electrochemical Hydrogen Oxidation and Evolution Reactions on the Basis of Density Functional Theory Calculations. *J. Phys. Chem. C* **2010**, *114*, 18182–18197.
- (16) Taylor, C.; Kelly, R. G.; Neurock, M. Theoretical Analysis of the Nature of Hydrogen at the Electrochemical Interface Between Water and a Ni(111) Single-Crystal Electrode. *J. Electrochem. Soc.* **2007**, *154*, F55–F64.
- (17) Das, R. K.; Wang, Y.; Vasilyeva, S. V.; Donoghue, E.; Pucher, I.; Kamenov, G.; Cheng, H.-P.; Rinzler, A. G. Extraordinary Hydrogen Evolution and Oxidation Reaction Activity from Carbon Nanotubes and Graphitic Carbons. *ACS Nano* **2014**, *8*, 8447–8456.
- (18) Deng, J.; Ren, P.; Deng, D.; Yu, L.; Yang, F.; Bao, X. Highly Active and Durable Non-Precious-Metal Catalysts Encapsulated in Carbon Nanotubes for Hydrogen Evolution Reaction. *Energy Environ. Sci.* **2014**, *7*, 1919–1923.

- (19) Hub, J. S.; de Groot, B. L.; Grubmüller, H.; Groenhof, G. Quantifying Artifacts in Ewald Simulations of Inhomogeneous Systems with a Net Charge. *J. Chem. Theory Comput.* **2014**, *10*, 381–390.
- (20) Andreussi, O.; Marzari, N. Electrostatics of Solvated Systems in Periodic Boundary Conditions. *Phys. Rev. B* **2014**, *90*, 245101.
- (21) Trasatti, S. The Absolute Electrode Potential: An Explanatory Note (Recommendations 1986). *Pure Appl. Chem.* **1986**, *209*, 417–428, 0022-0728.
- (22) Cheng, J.; Sprik, M. Alignment of Electronic Energy Levels at Electrochemical Interfaces. *Phys. Chem. Chem. Phys.* **2012**, *14*, 11245–11267.
- (23) Tripkovic, V.; Björketun, M. E.; Skúlason, E.; Rossmeisl, J. Standard Hydrogen Electrode and Potential of Zero Charge in Density Functional Calculations. *Phys. Rev. B* **2011**, *84*, 115452.
- (24) Fawcett, W. R. The Ionic Work Function and its Role in Estimating Absolute Electrode Potentials. *Langmuir* **2008**, *24*, 9868–9875.
- (25) Kelly, C. P.; Cramer, C. J.; Truhlar, D. G. Aqueous Solvation Free Energies of Ions and Ion-Water Clusters Based on an Accurate Value for the Absolute Aqueous Solvation Free Energy of the Proton. *J. Phys. Chem. B* **2006**, *110*, 16066–16081.
- (26) Kelly, C. P.; Cramer, C. J.; Truhlar, D. G. Single-Ion Solvation Free Energies and the Normal Hydrogen Electrode Potential in Methanol, Acetonitrile, and Dimethyl Sulfoxide. *J. Phys. Chem. B* **2007**, *111*, 408–422.
- (27) Isse, A. A.; Gennaro, A. Absolute Potential of the Standard Hydrogen Electrode and the Problem of Interconversion of Potentials in Different Solvents. *J. Phys. Chem. B* **2010**, *114*, 7894–7899.

- (28) Marenich, A. V.; Ho, J.; Coote, M. L.; Cramer, C. J.; Truhlar, D. G. Computational Electrochemistry: Prediction of Liquid-Phase Reduction Potentials. *Phys. Chem. Chem. Phys.* **2014**, *16*, 15068–15106.
- (29) Björketun, M. E.; Zeng, Z.; Ahmed, R.; Tripkovic, V.; Thygesen, K. S.; Rossmeisl, J. Avoiding Pitfalls in the Modeling of Electrochemical Interfaces. *Chem. Phys. Lett.* **2013**, *555*, 145–148.
- (30) Van de Walle, C. G.; Neugebauer, J. First-Principles Calculations for Defects and Impurities: Applications to III-Nitrides. *J. Appl. Phys.* **2004**, *95*, 3851–3879.
- (31) Leslie, M.; Gillan, N. The Energy and Elastic Dipole Tensor of Defects in Ionic Crystals Calculated by the Supercell Method. *J. Phys. C: Solid State Phys.* **1985**, *18*, 973, 0022-3719.
- (32) Makov, G.; Payne, M. C. Periodic Boundary Conditions in Ab Initio Calculations. *Phys. Rev. B* **1995**, *51*, 4014–4022.
- (33) Lany, S.; Zunger, A. Assessment of Correction Methods for the Band-Gap Problem and for Finite-Size Effects in Supercell Defect Calculations: Case Studies for ZnO and GaAs. *Phys. Rev. B* **2008**, *78*, 235104.
- (34) Freysoldt, C.; Neugebauer, J.; Van de Walle, C. G. Fully Ab Initio Finite-Size Corrections for Charged-Defect Supercell Calculations. *Phys. Rev. Lett.* **2009**, *102*, 016402.
- (35) Taylor, S. E.; Bruneval, F. Understanding and Correcting the Spurious Interactions in Charged Supercells. *Phys. Rev. B* **2011**, *84*, 075155.
- (36) Dabo, I.; Kozinsky, B.; Singh-Miller, N. E.; Marzari, N. Electrostatics in Periodic Boundary Conditions and Real-Space Corrections. *Phys. Rev. B* **2008**, *77*, 115139.
- (37) Schultz, P. A. Charged Local Defects in Extended Systems. *Phys. Rev. Lett.* **2000**, *84*, 1942–1945.

- (38) Rurali, R.; Cartoixà, X. Theory of Defects in One-Dimensional Systems: Application to Al-Catalyzed Si Nanowires. *Nano Lett.* **2009**, *9*, 975–979.
- (39) Hummer, G.; Pratt, L. R.; García, A. E. Ion Sizes and Finite-Size Corrections for Ionic-Solvation Free Energies. *J. Chem. Phys.* **1997**, *107*, 9275–9277.
- (40) Perdew, J. P.; Burke, K.; Ernzerhof, M. Generalized Gradient Approximation Made Simple. *Phys. Rev. Lett.* **1996**, *77*, 3865–3868.
- (41) VandeVondele, J.; Krack, M.; Mohamed, F.; Parrinello, M.; Chassaing, T.; Hutter, J. Quickstep: Fast and Accurate Density Functional Calculations Using a Mixed Gaussian and Plane Waves Approach. *Comput. Phys. Commun.* **2005**, *167*, 103–128.
- (42) Hutter, J.; Iannuzzi, M.; Schiffmann, F.; VandeVondele, J. CP2K: Atomistic Simulations of Condensed Matter Systems. *Wiley Interdiscip. Rev.: Comput. Mol. Sci.* **2014**, *4*, 15–25.
- (43) Guidon, M.; Hutter, J.; VandeVondele, J. Auxiliary Density Matrix Methods for Hartree-Fock Exchange Calculations. *J. Chem. Theory Comput.* **2010**, *6*, 2348–2364.
- (44) Guidon, M.; Hutter, J.; VandeVondele, J. Robust Periodic Hartree-Fock Exchange for Large-Scale Simulations Using Gaussian Basis Sets. *J. Chem. Theory Comput.* **2009**, *5*, 3010–3021.
- (45) Grimme, S.; Antony, J.; Ehrlich, S.; Krieg, H. A Consistent and Accurate Ab Initio Parametrization of Density Functional Dispersion Correction (DFT-D) for the 94 Elements H-Pu. *J. Chem. Phys.* **2010**, *132*, 154104–19.
- (46) VandeVondele, J.; Hutter, J. Gaussian Basis Sets for Accurate Calculations on Molecular Systems in Gas and Condensed Phases. *J. Chem. Phys.* **2007**, *127*, 114105–9.
- (47) Goedecker, S.; Teter, M.; Hutter, J. Separable Dual-Space Gaussian Pseudopotentials. *Phys. Rev. B* **1996**, *54*, 1703–1710.
- (48) Hartwigsen, C.; Goedecker, S.; Hutter, J. Relativistic Separable Dual-Space Gaussian Pseudopotentials from H to Rn. *Phys. Rev. B* **1998**, *58*, 3641–3662.

- (49) Krack, M. Pseudopotentials for H to Kr Optimized for Gradient-Corrected Exchange-Correlation Functionals. *Theor. Chem. Acc.* **2005**, *114*, 145–152.
- (50) Srivastava, D.; Susi, T.; Borghei, M.; Laasonen, K. Dissociation of Oxygen on Pristine and Nitrogen-Doped Carbon Nanotubes: A Spin-Polarized Density Functional Study. *RSC Adv.* **2014**, *4*, 15225–15235.
- (51) Nosé, S. A Unified Formulation of the Constant Temperature Molecular Dynamics Methods. *J. Chem. Phys.* **1984**, *81*, 511–519.
- (52) Swope, W. C.; Andersen, H. C.; Berens, P. H.; Wilson, K. R. A Computer Simulation Method for the Calculation of Equilibrium Constants for the Formation of Physical Clusters of Molecules: Application to Small Water Clusters. *J. Chem. Phys.* **1982**, *76*, 637–649.
- (53) Henkelman, G.; Uberuaga, B. P.; Jónsson, H. A Climbing Image Nudged Elastic Band Method for Finding Saddle Points and Minimum Energy Paths. *J. Chem. Phys.* **2000**, *113*, 9901–9904.
- (54) Barone, V.; Peralta, J. E.; Uddin, J.; Scuseria, G. E. Screened Exchange Hybrid Density-Functional Study of the Work Function of Pristine and Doped Single-Walled Carbon Nanotubes. *J. Chem. Phys.* **2006**, *124*, 024709.
- (55) Barisci, J. N.; Wallace, G. G.; Chattopadhyay, D.; Papadimitrakopoulos, F.; Baughman, R. H. Electrochemical Properties of Single-Wall Carbon Nanotube Electrodes. *J. Electrochem. Soc.* **2003**, *150*, 409–415.
- (56) Nørskov, J. K.; Bligaard, T.; Logadottir, A.; Kitchin, J. R.; Chen, J. G.; Pandelov, S.; Stimming, U. Trends in the Exchange Current for Hydrogen Evolution. *J. Electrochem. Soc.* **2005**, *152*, 23–26.
- (57) Greeley, J.; Jaramillo, T. F.; Bonde, J.; Chorkendorff, I.; Nørskov, J. K. Computational High-

- Throughput Screening of Electrocatalytic Materials for Hydrogen Evolution. *Nat. Mater.* **2006**, *5*, 909–913.
- (58) Zhang, Z.; Cho, K. Ab Initio Study of Hydrogen Interaction with Pure and Nitrogen-Doped Carbon Nanotubes. *Phys. Rev. B* **2007**, *75*, 075420.
- (59) Li, D. J.; Maiti, U. N.; Lim, J.; Choi, D. S.; Lee, W. J.; Oh, Y.; Lee, G. Y.; Kim, S. O. Molybdenum Sulfide/N-Doped CNT Forest Hybrid Catalysts for High-Performance Hydrogen Evolution Reaction. *Nano Lett.* **2014**, *14*, 1228–1233.
- (60) Zou, X.; Huang, X.; Goswami, A.; Silva, R.; Sathe, B. R.; Mikmeková, E.; Asefa, T. Cobalt-Embedded Nitrogen-Rich Carbon Nanotubes Efficiently Catalyze Hydrogen Evolution Reaction at All pH Values. *Angew. Chem.* **2014**, *126*, 4461–4465.
- (61) Cui, W.; Liu, Q.; Cheng, N.; Asiri, A. M.; Sun, X. Activated Carbon Nanotubes: A Highly-Active Metal-Free Electrocatalyst for Hydrogen Evolution Reaction. *Chem. Commun.* **2014**, *50*, 9340–9342.
- (62) Skúlason, E.; Karlberg, G. S.; Rossmeisl, J.; Bligaard, T.; Greeley, J.; Jónsson, H.; Nørskov, J. K. Density Functional Theory Calculations for the Hydrogen Evolution Reaction in an Electrochemical Double Layer on the Pt(111) Electrode. *Phys. Chem. Chem. Phys.* **2007**, *9*, 3241–3250.
- (63) Usachov, D.; Vilkov, O.; Grüneis, A.; Haberer, D.; Fedorov, A.; Adamchuk, V. K.; Preobrajenski, A. B.; Dudin, P.; Barinov, A.; Oehzelt, M. et al. Nitrogen-Doped Graphene: Efficient Growth, Structure, and Electronic Properties. *Nano Lett.* **2011**, *11*, 5401–5407.

Graphical TOC Entry

